Inorganic Chemistry Communications 165 (2024) 112557

Contents lists available at ScienceDirect

Inorganic Chemistry Communications

journal homepage: www.elsevier.com/locate/inoche

Short communication

Monoclinic α-Bi_2O_3 nanorods by microwave-assisted synthesis: Photocatalytic and antioxidant properties

Marwa Yousry A. Mohamed [a], Hela Ferjani [b,*], Opeyemi A. Oyewo [c], Oluwasayo E. Ogunjinmi [d], Seham M. Hamed [a], Chahra Amairia [e], Seshibe Makgato [c], Damian C. Onwudiwe [f,g,**]

[a] Biology Department, College of Science, Imam Mohammad Ibn Saud Islamic University (IMSIU), Riyadh 11623, Saudi Arabia
[b] Chemistry Department, College of Science, Imam Mohammad Ibn Saud Islamic University (IMSIU), Riyadh 11623, Saudi Arabia
[c] Department of Chemical Engineering, College of Science, Engineering and Technology, University of South Africa (UNISA), Florida Campus 1710, Johannesburg, South Africa
[d] Department of Industrial Chemistry, First Technical University Ibadan, Nigeria
[e] Chemistry Department, College of Science, Al-Baha University, Al Bahah 65779, Saudi Arabia
[f] Materials Science Innovation and Modelling (MaSIM) Research Focus Area, Faculty of Natural and Agricultural Science, North-West University, Private Bag X2046, Mmabatho, South Africa
[g] Department of Chemistry, Faculty of Natural and Agricultural, Science, North-West University (Mafikeng Campus), Private Bag X2046, Mmabatho 2735, South Africa

ARTICLE INFO

Keywords:
Microwave synthesis
Bismuth oxide
Nanostructures
Photocatalysis
Radical scavenging

ABSTRACT

Nanotechnology has emerged as a new route for addressing most environmental and medical challenges, hence this field of research continues to generate research interest. Herein, Bi_2O_3 was synthesized by a microwave-assisted thermal process. X-ray diffraction (XRD) result confirmed that a nanocrystalline monoclinic crystal structure of the α-phase was formed, and both the Scanning Electron Microscopy (SEM) and Transmission Electron Microscopy (TEM) analysis confirmed that the synthesized α-Bi_2O_3 were rod-like in shape. The length of the nanorods was in the range of 60–160 nm, with an average dimension of 101.5 nm, while the width has an average value of 23 nm. A band gap energy value of 2.75 eV was obtained from the absorption spectroscopy, and they absorbed light in the UV to visible range, with an absorption maximum of around 345 nm. Photocatalytic activity of the nanorods under UV irradiation was investigated by assessing the degradation of Bromocresol green (BG) as a model pollutant. The degradation process of the dye molecules was studied at different concentrations (20–80 mg/L), varied photocatalyst dosage (0.025, 0.05, 0.075, and 1.0 g), and a range of solution pH (3, 6, 9, and 12). About 75 % optimum photocatalytic efficiency was achieved at pH 6 after 3 h. In addition, the results showed that an increase in catalyst dosage and concentration of dye molecules contributed to promoting the degradation effect. Moreover, the photocatalyst was found to be stable after 4 consecutive cycles, with negligible loss of efficiency. The antioxidant potency of the nanorods was assessed by evaluating their free radical scavenging capabilities across 4 different assays: 1,1-diphenyl-2-picrylhydrazyle (DPPH), Nitric oxide (NO), Hydrogen peroxide (HP) radical inhibition, and Reducing power (RP). The results from the IC_{50} values indicated the sample exhibited better inhibition of HP (25.22 μg/mL), followed by RP (28.22 μg/mL), NO (29.37 μg/mL), and DPPH (32.72 μg/mL) respectively. However, the standard Ascorbic acid exhibited IC_{50} values of 16.25, 24.50, 25.07, and 28.40 μg/mL for DPPH, RP, HP, and NO, respectively. These unique properties of the nanorods showed that they have good antioxidant potential that is comparable with that of Ascorbic acid used as the standard.

1. Introduction

The utilization of nanocrystalline materials in photocatalytic water treatment is a widely recognized advanced oxidation method (AOP) employed in environmental remediation [1,2]. Through the creation of electron-hole pairs under light exposure, nanomaterials can break down

* Corresponding author.
** Corresponding author at: Materials Science Innovation and Modelling (MaSIM) Research Focus Area, Faculty of Natural and Agricultural Science, North-West University, Private Bag X2046, Mmabatho, South Africa.
E-mail addresses: hhferjani@imamu.edu.sa (H. Ferjani), Damian.Onwudiwe@nwu.ac.za (D.C. Onwudiwe).

https://doi.org/10.1016/j.inoche.2024.112557
Received 7 March 2024; Received in revised form 4 May 2024; Accepted 14 May 2024
Available online 17 May 2024

various organic compounds, transforming them into non-hazardous byproducts such as carbon dioxide, water, and some inorganic ions [3]. This photo-enhanced catalytic destruction of contaminants by nanomaterials in aqueous solutions is mainly promoted by a sequence of hydroxylation reactions which are initiated by hydroxyl radicals ($^{\bullet}OH$) [4–7].

When semiconductor nanomaterials are exposed to light of sufficient energy (equals or exceeds the material's band gap), they generate electron-hole pairs. Electrons (e^-) get excited from the semiconductor's valence band (VB) to the conduction band (CB), resulting in the creation of a positive hole (h^+) in the valence band. This stimulation of charge carriers (e^-/h^+) marks the onset of the photocatalytic degradation process. The positive hole in the valence band facilitates the oxidation of surface-absorbed water molecules or OH^-, thereby generating hydroxyl radicals ($^{\bullet}OH$). Simultaneously, the photoexcited electrons reduce oxygen molecules, yielding hydroperoxyl radicals ($HO_2^{\bullet}$) or superoxide radicals ($^{\bullet}O_2^-$)[8]. Consequently, all these species collaborate in the generation of $^{\bullet}OH$, which subsequently targets and attacks the pollutants within the water solution [3]. Among the semiconductor photocatalysts, metal oxides have been widely used because of their good stability, environmental friendliness, and availability [9]. Bismuth oxide (Bi_2O_3) has been widely studied due to its several positive features including significant band gap energy, high photoconductivity, and enhanced refractive index [10,11].

One of the characteristic features of bismuth oxide is its polymorphism, exhibiting five different modifications: α-, β-, γ-, δ-, and ω-Bi_2O_3 [12,13]. Two of these polymorphs: the α and δ phases are stable at low and high temperatures respectively, while the rest are metastable at high temperatures [13]. Each of these polymorphs possesses unique crystalline structures and distinct physical properties including good optical, high electrical, and photoelectrical properties. The monoclinic α-Bi_2O_3 exhibits a band gap of 2.85 eV at 300 K, while the tetragonal β phase has a band gap of 2.58 eV [10]. Bismuth oxide have mostly been reported as ID nanostructures [14–18].

in the proximity of the grain boundaries actively alters the electrical transport properties within polycrystalline materials [19]. Moreover, as the width of the nanorod decreases, the finite size of the rod imposes constraints on electron wave functions. This confinement results in the establishment of quantized energy levels, leading to significant modifications in both the electrical transport as well as the optical characteristics of the material [10].

Apart from radical generation in photocatalysis and its application in water treatment, semiconductor nanomaterials have recently emerged as crucial and cutting-edge materials for the development of advanced alternatives both for drug delivery, diagnostic and therapeutic applications for diseases such as cancer and infectious disorders [20–22]. Oxidative stress induced by free radicals stands as the primary cause of various diseases and conditions, including neurological disorders, aging, and cancer [23]. These free radicals instigate cellular damage and disrupt homeostasis by engaging with proteins, nucleic acids, and lipids. Antioxidants play a pivotal role in shielding the cells and large biological molecules by scavenging the free radicals and diminishing the generation of reactive oxygen species (ROS) [24–26]. Nanoparticles have cytotoxic effects against cancerous cells and can neutralize free radicals thereby acting as antioxidants [25].

Herein, a microwave-enhanced hydrothermal method is devised for the preparation of Bi_2O_3 nanorods. Microwave-assisted methods offer several advantages, including rapid reaction kinetics, high purity, uniform size distribution, enhanced crystallinity, and tuneable morphologies. These advantages of microwave synthesis make it desirable when compared to other conventional methods. For example, Bi_2O_3 nanoparticles prepared using an aqueous extract of plant were only successful after 24 h at 90 °C [27]. Bi_2O_3 nanowires were prepared using a combination of sol–gel process and electrospinning methods, and the process was followed by calcination process in the air at 400 °C and 600 °C for 3 h [28]. The microwave-synthesized nanorods were characterized by different analytical techniques including XRD, UV–vis spectroscopy, TEM and SEM measurements. The results showed nanorods with a unique monoclinic crystal structure, which has the potential of imparting exceptional photocatalytic and antioxidant properties, making them promising candidates for various environmental and biomedical applications.

Hence, the photocatalytic property of the fabricated nanorod was evaluated by studying the photodegradation of Bromocresol green (BG) as model pollutant in aqueous solution under ultraviolet light illumination. Additionally, the antioxidant activity was assessed and the nanorods showed very good free radical scavenging efficacy in all the assays used to assess its antioxidant activity including nitric oxide scavenging, Hydrogen peroxide (HP), Reducing power (Ferric reducing power) and DPPH free radicals scavenging assays. This is the first report on the photocatalytic and antioxidant studies of Bi_2O_3 nanorods obtained from microwave route, and it offers the potential of extension to other similar metal oxides.

2. Experimentals

2.1. Materials and methods

All the chemical reagents used in this study were commercially obtained and were used as received without any purification treatment. Bismuth nitrate pentahydrate, $Bi(NO_3)_3{\cdot}5H_2O$, ethylenediamine (En, 99 %), sodium hydroxide were purchased from ACE Chemicals, while DPPH (2,2-diphenyl-1-picrylhydrazyl), Bromocresol green (BG), hydrogen peroxide (HP), sodium nitroprusside, ascorbic acid, and potassium ferricyanide, and phosphate buffer were obtained from Merck chemicals.

2.2. Synthesis of Bi_2O_3 nanorods

In a typical synthesis procedure, 20 mL ethanol solution of Bi $(NO_3)_3{\cdot}5H_2O$ (1.5 mmol) was added to 5 mL of ethylenediamine (En, 99 %) and stirred for about 30 min. Sodium hydroxide solution was added dropwise to adjust the pH of the solution to 8. Thereafter, the solution was transferred into a 50 mL microwave reactor vessel and heated at 160 °C for 5 min under microwave radiation. The product obtained was cooled to room temperature, rinsed several times with distilled water and followed with ethanol, before drying at 80 °C for 10 h. The dried product was further calcined for 2 h at 400 °C.

2.3. Characterization methods

A Bruker D8 Advanced XRD diffractometer was used to measure the sample's crystallinity and composition. UV–visible diffuse reflectance (DRS) spectrum was recorded using Thermo scientific evolution 300 UV–visible spectrophotometer. FEI QUANTA FEG-200 scanning electron microscope was used to visualize the particle surface morphology, while the internal morphology was analyzed on a JEM-3010 transmission electron microscope. The materials' surface charge was assessed by measuring their zeta potential with a Malvern Nano ZS instrument.

2.4. Photocatalysis studies

The degradation of an aqueous solution of BG under visible light irradiation was used to assess the photocatalytic activity of the Bi_2O_3 nanorods. A 250-W Xe discharge lamp with a recirculating water source in the reactor vessel and a dye concentration of 20 mg/L was created for the investigation. To create an adsorption equilibrium between the catalysts' and the dye's surfaces, 0.075 g of the nanorods were added to the dye solution for each measurement, and the mixture was magnetically agitated for an hour while the light was off. After that, the suspension was continuously stirred for 3 h under the lamp. Aliquots of the solution were taken during this procedure at 15-min intervals.

UV–visible spectroscopy was used to investigate the dye's degradation efficiency.

2.5. Antioxidant assay

The antioxidant activity of the nanorod was assessed by four (4) different assays as follows:

2.5.1. 1,1-diphenyl-1-picrylhydrazyl) (DPPH)

The antioxidant activity of nanoparticles has been extensively measured using the DPPH scavenging assay [29,30]. In the current study, the scavenging of the free radicals generated by 1,1-diphenyl-1-picrylhydrazyl (DPPH) was utilized to assess the free radical scavenging activity of the nanorods and Ascorbic acid (AA) used as the positive control. Six different concentrations (1.56 – 50 μg/mL) of the two samples (Bi_2O_3 and AA) were prepared and 1 mL of 0.1 mM DPPH in 100 percent ethanol was added to each concentration. The solutions were analysed after a 30 min incubation period at room temperature in the dark. The measurement was conducted by sampling 250 μL of each solution into a 96-well microplate in triplicates and measuring the absorbance at 517 nm in comparison with the measurement of a blank solution. The percentage of free radical scavenging activity was estimated using equation (1):

$$\%\ \text{scavenged DPPH}\ (\%) = \frac{A_o - A_t}{A_o} \quad (1)$$

Where A_o represents the absorbance of the control at 30 min and A_t is the absorbance of Bi_2O_3.

2.5.2. Nitric oxide (NO) assay

The approach for investigating the nitric oxide scavenging assay followed a previously reported procedure [31]. Specifically, sodium nitroprusside (2 mL, 10 mM) was combined with the respective solutions of the nanorods in phosphate-buffered saline (0.5 mM; pH 7.4) and maintained at 25 °C for 4 h. Subsequently, the solution containing the nanorods or the standard ascorbic acid (AA) of approximately 0.5 mL was mixed with Griess reagent and left at 25 °C for 30 min. These mixed solutions were then pipetted into a 96-well microplate, and their absorbance was measured at an absorption wavelength of 540 nm. This entire experiment was repeated three times for each solution of the nanorod and AA. The percentage of scavenging properties was calculated using equation (2).

$$\%\ \text{scavenged}\ [\text{NO}] = \frac{[\text{Ab} - \text{As}]}{\text{Ab}} \text{X}\,100 \quad (2)$$

Ab = absorbance of the blank; As = absorbance of the nanorods or AA. The IC_{50}, representing the concentration at which 50 % inhibition occurred, was determined by analyzing the plot correlating the percentage of inhibition with concentration.

2.5.3. Hydrogen peroxide (HP) assay

Approximately 5 mL of the Bi_2O_3 nanorods or AA was dissolved in a 1 % solution and subjected to serial dilution ranging from 50 to 1.56 μM. These resulting solutions were combined with 0.5 mL of H_2O_2 prepared within a phosphate buffer (0.1 M: pH 7.4) and allowed to incubate at 25 °C for 10 min. Subsequently, utilizing an automatic pipette, these prepared samples (250 μL each) were transferred into a 96-well microplate, and their absorbance at 405 nm was gauged [32]. Following this, the percentage of scavenging properties of the samples was computed using equation (3).

$$\%\ \text{scavenged}\ [H_2O_2] = \frac{[\text{Ab} - \text{As}]}{\text{Ab}} \text{X}\,100 \quad (3)$$

Ab = absorbance of the blank; As = absorbance of the nanorods or AA.

2.5.4. Reducing power assay (Ferric reducing power)

Approximately 0.3 mL of the different samples (Bi_2O_3 and AA) concentrations were mixed with an equal concentration of potassium ferricyanide and phosphate buffer. The solutions were sonicated, followed by incubation at 50 °C. Upon reaching 25 °C, 0.2 mL of 10 % trichloroacetic acid was introduced, and the mixture was centrifuged at 4500 rpm for 15 min. Subsequently, 100 μL was extracted from this mixture and combined with ferric chloride (20 μL) and distilled water (100 μL). The absorbance at 700 nm was measured after transferring the solution into a 96-well microplate [33]. This entire process was repeated three times.

3. Results and discussion

3.1. Structural and morphological properties

The particles' crystalline structure was studied by using powder X-ray diffraction measurement and the pattern is presented in Fig. 1. The diffraction patterns indicate that the major characteristic peaks identified around 21.72°, 24.56°, 25.80°, 26.92°, 27.38°, 28.02°, 33.23°, 35.01°, 37.65°, 46.35°, 48.62°, 54.80°, 55.45°, 63.56° and 71.39° could be ascribed to the (−111), (020), (−102), (002), (−112), (−121), (−202), (−212), (−113), (041), (−104), (−241), (−224), (−115) and (−161) lattice planes of monoclinic crystal structure of α-Bi_2O_3 and correspond to the standard card JCPDS NO. 71-2274 [34]. This phase of Bi_2O_3 belong to the space group $P21/c$, and has lattice constants of a = 5.850 Å, b = 8.170 Å, c = 7.512 Å [34]. The two predominant peaks were observed at 2θ values of 27.3° and 33.2° with d-spacings of 3.25 Å and 2.71 Å, respectively, indicating the presence of the (−112) and (−202) reflection planes of Bi_2O_3 [35]. The average crystallite sizes of Bi_2O_3 nanorods were calculated from these two most prominent peaks

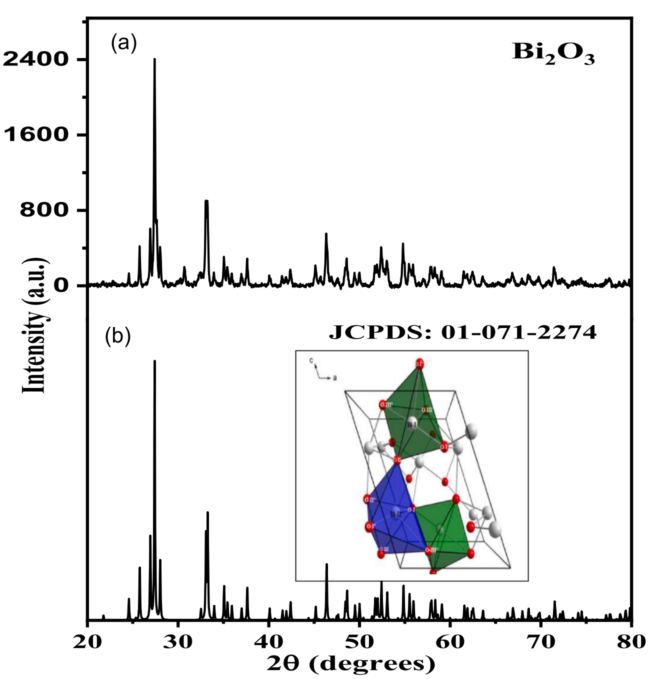

Fig. 1. (a) XRD pattern of the synthesized α-Bi_2O_3 nanorods, (b) standard pattern for the standard card JCPDS NO. 71-2274 (inset is the arrangement of monoclinic crystalline structure of α-Bi_2O_3 under standard pressure, viewed from the perspective of the (0 $\bar{1}$ 0) plane. Bi atoms are depicted as gray balls, while O atoms are represented by red balls. This structure displays one Bi atom surrounded by five coordinating entities (Bi–I—illustrated by green polyhedra) and another Bi atom surrounded by six coordinating entities (Bi–II—depicted by blue polyhedra) [37]. (For interpretation of the references to color in this figure legend, the reader is referred to the web version of this article.)

by the Scherrer equation (4) and determined to be 34 nm.

$$D = K\lambda/\beta Cos\,\theta \quad (4)$$

where D is the crystallite size, K is the Scherrer constant, λ is obtained from the wave length of the X-ray beam used (1.54,184 Å). The value of β gives the Full width at half maximum (FWHM) of the peak and θ is the Bragg angle [36]. Scherrer constant, denoted by K, represents the shape of the particle and its value is often taken as 0.9.

To examine the morphology, the synthesized α-Bi_2O_3 nanorods were studied by SEM and TEM analyses, and the obtained micrographs are presented in Fig. 2. The SEM images in Fig. 2(a) and (b) are the product before and after calcination respectively, and they revealed the transformation of the polymeric and irregular shape of the precursor material after microwave irradiation (Fig. 2a) to the monoclinic α-Bi_2O_3 nanomaterials possessing rod-shaped morphologies (Fig. 2b) after calcination. It is interesting to observe how the nanorods are grown in very high density. Fig. 2c presents the TEM images of the monoclinic α-Bi_2O_3, confirming the rod-shaped morphology. The HRTEM image of Fig. 2d exhibits distinct fringes with a lattice spacing of 3.03 Å and 2.74 Å. These could be indexed to the (211) and (012) crystal planes of

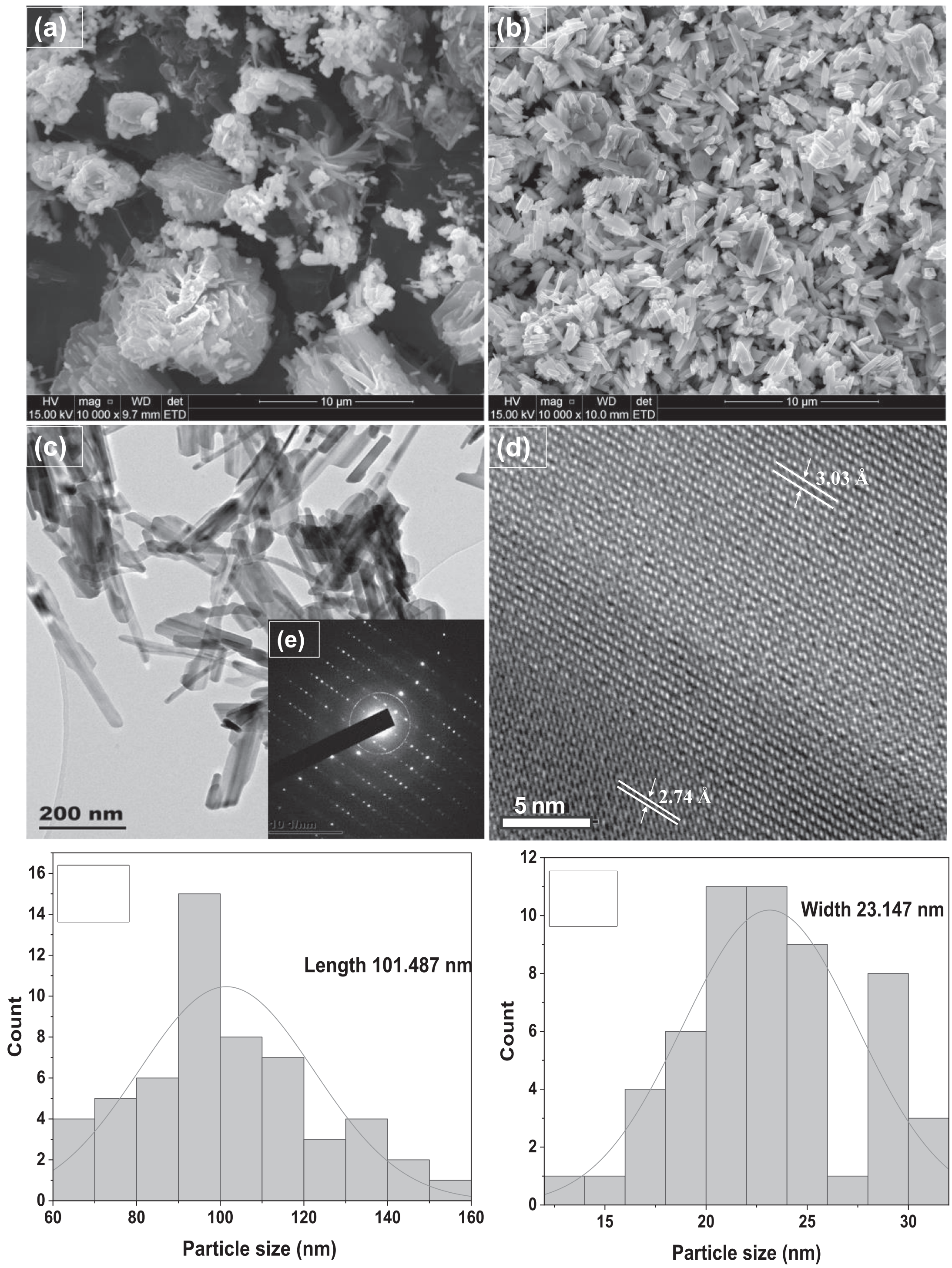

Fig. 2. SEM images of (a) precursor to the monoclinic α-Bi_2O_3, and (b) monoclinic α-Bi_2O_3; (c) TEM, (d) HRTEM, (e) The SAED, and particle size distribution histogram showing (e) length and (f) width of image of monoclinic α-Bi_2O_3.

monoclinic α-Bi_2O_3 respectively [38], and indicate that the results from HRTEM are in consonant with the XRD results. Also, the selected area electron diffraction (SAED) pattern is presented in Fig. 3, which also confirms a single-crystal structure for the α-Bi_2O_3 [39]. The length of the nanorods is in the range of 60–160 nm, with an average dimension of 101. 5 nm (Fig. 2e), while the width has an average value of 23 nm (Fig. 2f). This indicates that the nanorods possess a high-aspect ratio. Apart from their high-aspect ratio, it could also be observed from the TEM micrographs that the nanorods possess smooth surfaces throughout their lengths, which reveals a full consistency between the SEM and TEM results in terms of morphologies and dimensionality.

3.2. Optical properties

The optical property of a semiconductor indicates the position of absorption in the solar spectrum and it is recognized as a critical factor that determines its photocatalytic ability [40]. The optical absorption is related to the energy band structure of the material, and this has been measured using the diffuse reflection adsorption spectra (DRS) as shown in Fig. 3. The α-Bi_2O_3 present significant absorption properties spanning from the UV- to visible range of light with absorption edge located at 475 nm, similar to previous report [38]. The band gap energy value was analysed using the classical relation that describes a near edge optical absorption in semiconductors, which is given as equation (5):

$$\alpha = A(h\nu - E_g)^{n/2}/h\nu \quad (5)$$

where A is a constant, E_g is the band gap energy value of the semiconductor and n is a number which is dependent on the type of semiconductor (it is equal to 1 for direct gap and 4 for indirect gap semiconductors). The plots of $(\alpha h\nu)^2$ vs $h\nu$ of the α-Bi_2O_3 is shown in the inset of Fig. 3, and the extrapolation of the tangent curve to zero absorption coefficient gives the optical band gap energy 2.75 eV, which is very close to band gap value of monoclinic Bi_2O_3 (2.85 eV) [41].

3.3. Photodegradation of bromocresol green using Bi_2O_3 nanorods

The photocatalytic activity of the produced Bi_2O_3 nanorods was determined under visible light irradiation using 20 mg/L solution of bromocresol green (BG) dye and 0.075 g of catalyst at pH 6. A UV–vis spectrophotometer was used to determine the residual BG concentration. After exposure to visible light for 180 min, the dye solution began to progressively lose its color. An aliquot was sampled every 15 min. The dye was found to undergoe sequential degradation as exhibited in the steady decrease in the peak position at about 415 and 620 nm [42], which are the maximum absorption wavelength typical of BG. The position of the greatest absorption peak was found to remain constant throughout the analysis procedure, indicating that the examined solution was free of any contaminants. Additionally, during the photocatalytic process, the dye solution's color varied from green to colourless suggesting a decrease in the concentration of BG. The acquired spectra line, which is shown in Fig. 4, revealed that the BG was gradually degrading over time, eventually reaching practically full degradation of 75 %. Bi_2O_3 nanorods are anticipated to increase this activity, as they act as a co-catalyst thereby prolonging the recombination of the charge carriers within the system [43].

3.3.1. Photocatalytic activity of Bi_2O_3 NPs as a function of surface charges

The zeta potential is a measure of a nanoparticle's electrical charge within its environment. In aqueous solutions, nanoparticles typically bear a positive, negative, or neutral charge. Surface-modified nanoparticles acquire their charge through the dissociation of acidic or basic groups on their surfaces, resulting in negative or positive charges, respectively. In contrast, unmodified nanoparticles derive their charge from the constituent atoms on their surfaces [44]. Modifying the pH of a medium containing nanoparticles can lead to variations in its dissolution into ions or modify the surface chemistry [45]. This alteration in surface chemistry can influence the nanoparticle's interactions with both organic and inorganic pollutants, potentially impacting photocatalytic mechanisms. Moreover, alongside pH adjustments, the zeta potential of a nanoparticle shifts over time while suspended in aqueous solution. Examining the surface charge of nanoparticles is crucial because various water sources in the environment are known to exhibit differing pH levels. Given that photocatalysis takes place on the surface of these nanoparticles, the efficiency of the photocatalyst is significantly impacted by the pH of the solution [46,47], the type of pollutants present, and the surface's capacity to adsorb pollutants [48]. Therefore, identifying the point of zero charge (pHPZC) plays a crucial role in anticipating the surface charge of nanoparticles during the photodegradation process [49].

Figure 5 illustrates the Zeta potential of Bi_2O_3 nanoparticles in relation to the pH of the solution. The graph highlights the point of zero charge (pHPZC) for Bi_2O_3 nanoparticles synthesized at pH levels of 3.0, 6.0, 9.0, and 12.0, which were determined to be 6.80, 5.85, 4.73, and 4.25, respectively. Below the pHPZC, the nanoparticles exhibited a

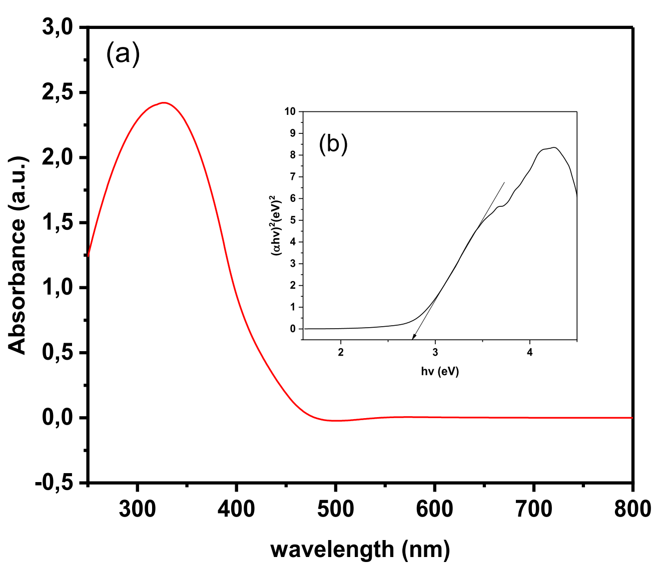

Fig. 3. (a) Absorption spectrum of the synthesized α-Bi_2O_3 nanorods (inset is the Tauc plot indicting the value of the band gap energy).

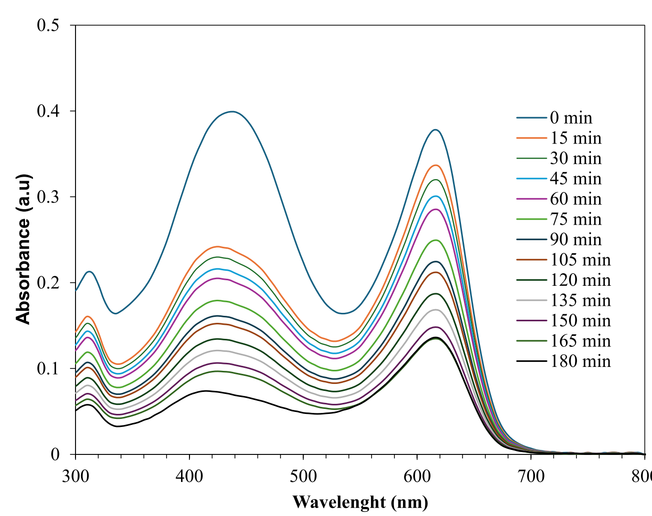

Fig. 4. The absorption spectra of aqueous solution of bromocresol green (BG) and photocatalyst measured at 15 min intervals. (For interpretation of the references to color in this figure legend, the reader is referred to the web version of this article.)

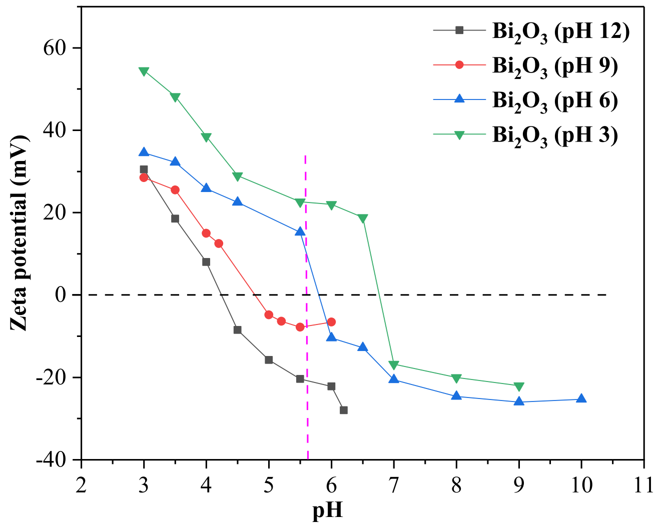

Fig. 5. Zeta potential measurements of Bi_2O_3 nanoparticles prepared at different solution pH of 3,6,9, and 12,

positive charge, whereas higher pH levels led to the development of negative charges on the nanoparticles [49].

3.3.2. Effect of solution pH

The solution pH has been reported an impact on the degree of ionization and the surface chemistry of the catalysts; therefore, it is crucial for the photocatalysis process [50]. Photocatalytic degradation studies of the BG dye (pH = 5.65) in an aqueous suspension of the Bi_2O_3 nanoparticles, which were prepared at varying pH values were conducted to evaluate their photocatalytic activity. Hence, about 20 mg/L of BG was examined at various solution pH values (3–12), as shown in Fig. 6. The solution pH 6 exhibited the highest degradation percentage of 74.5 %, which was followed by pH 3. The notable efficiencies observed in Bi_2O_3 nanoparticles produced at pH levels of 6.0 and 3 are likely due to the presence of positive charges on their surfaces. Consequently, the negatively charged anionic dye BG can be effectively absorbed onto the highly positively charged surface of Bi_2O_3 nanoparticles, facilitated by a robust electrostatic attraction. This electrostatic interaction plays a pivotal role in improving the adsorptive capabilities, thereby augmenting degradation efficiencies, as demonstrated in the instances of Bi_2O_3 nanoparticles prepared at pH 6.0 and 3.0. The graph shows that a pH increases from 9 to 12 displayed a noticeable decrease in the degradation of BG. This may be ascribed to the effect of reduction in some positively charged sites under alkaline conditions, which in turn caused a reduction in the degradation of the anionic dye [51]. Similar observations have been reported in previous studies related to Bi_2O_3 nanorods [43,52].

3.3.3. Effect of catalyst dosage

Different catalyst loadings of 0.025, 0.05, 0.075, and 1.0 g, were utilized to ascertain the correlation between the catalyst dosage and the percentage of BG degradation. As shown in Fig. 7, the degradation efficiency increased with an increase in catalyst dosage. This is because the number of active sites on the nanocatalyst increased, leading to the production of more active radicals (superoxide and hydroxyl), that initiated the degradation process. Furthermore, an increase in the catalyst loading is equivalent to a high concentration of photons absorbed and improved adsorption of high concentration of dye molecules [53]. The increased rate is a result of the increased particle density in the illuminated area. Another possibility is the paucity in the substrate molecules accessible for photocatalysis due to an increase of particles at a particular level [54,55]. Consequently, the extra 1.0 g of catalyst powder did not impact on the catalyst's activity, and the rate did not rise as the catalyst's concentration increased above 0.75 g. However, as the catalyst dosage increased further, a decreasing trend was observed in the degradation performance. Therefore, further studies on the degradation process involving the Bi_2O_3 nanorods utilized 0.075 g as the optimum dosage for all the experiments.

3.3.4. Effect of initial concentration of the BG dye

The influence of the initial concentration of BG was carried out at pH 4 using 0.075 g of the photocatalyst and various BG concentrations ranging from 20 to 80 mg/L in order to achieve the optimal starting concentration of BG dye. The effect of the initial concentration of dye molecules on the photocatalytic breakdown is shown in Fig. 8. Degradation was attained using an initial BG dye concentration of 20 mg/L. When the initial BG concentration is greater than 20 mg/L, the degradation percentage tends to decrease. This could be as a result of the increased concentration dye molecules impeding the incident radiation of the light from surface of the photocatalyst, hence serving as the inner filter [56]. The increased dye concentration prevents the photogenerated holes, superoxide, and hydroxyl radicals from directly contacting the substrate. In addition, more dye molecules are deposited on the surface of the photocatalyst, obstructing its active sites[53]. Other

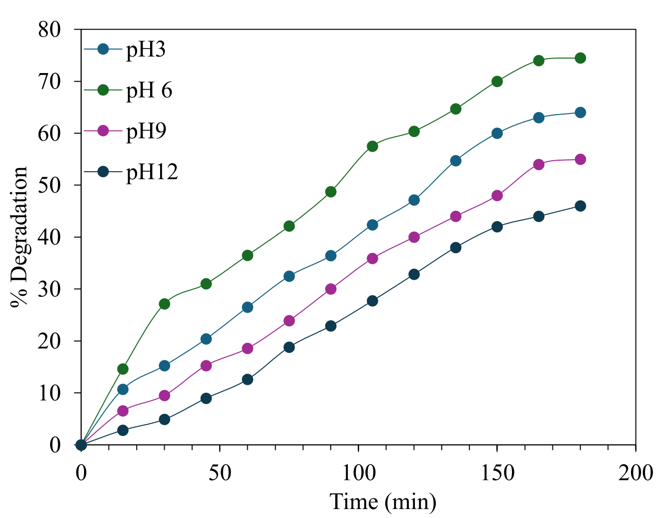

Fig. 6. The effect of pH on the photo degradation of BG using Bi_2O_3 nanorods (Initial concentration 20 mg/L; catalyst loading 0.75 g/L; radiation time 180 min).

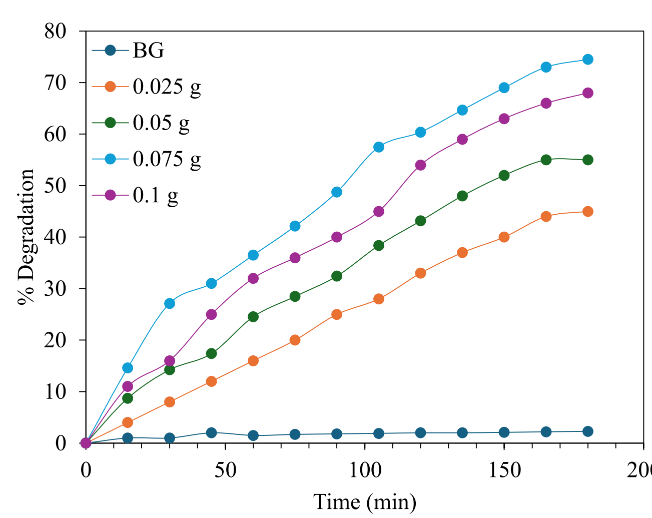

Fig. 7. The effect of catalyst loading on the photo degradation of BG using Bi_2O_3 nanorods (Initial concentration 20 mg/L; solution pH 6; radiation time 180-min).

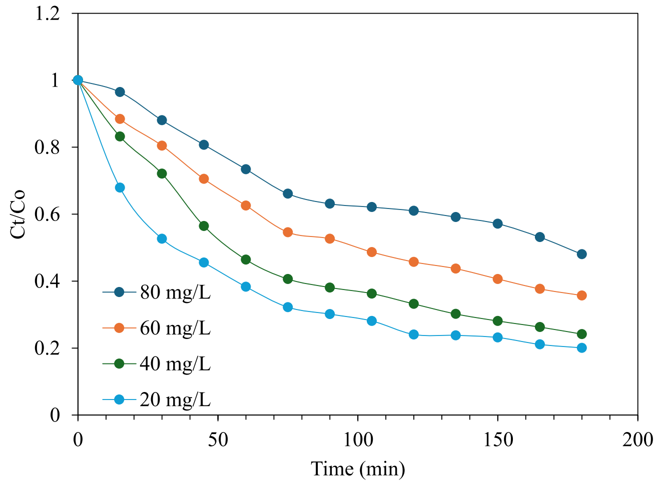

Fig. 8. Effect of initial concentration on the photocatalytic degradation of BG using Bi_2O_3 nanorods (catalyst dosage. 0.075 g/L, pH. 6).

factors that may contribute to the reduction in the efficiency of degradation (with increase in the starting concentration) include the absorption of a sizable portion of light radiation by more of the dye molecules rather than the catalyst, a reduction in photon path length, and a decline in the ratio of OH radicals to the dye molecules [57]. Bi_2O_3 nanorods are potential photocatalyst suitable for the degradation of pollutants in very low concentrations in an aqueous solution. The photocatalytic efficiency of the investigated Bi_2O_3 nanorods has been compared with other relevant binary nanoparticles that have been evaluated on BG dye in literature and presented in Table 1. The high efficiency of the Bi_2O_3 reported in the current study establishes the potential application of the Bi_2O_3 nanorods as photocatalysts.

In order to determine the resilience of this photocatalyst, reusability and photo stability experiments were conducted on the spent Bi_2O_3 nanorods. The outcome of the repeated 20 mg/L BG reduction using the as-prepared 0.075 g/L photocatalyst is shown in Fig. 9. Bi_2O_3 nanorods showed minimal reduction in activity even after four consecutive cycles of recyclability evaluation, indicating that it can be reused at least four times[64]. The activity appears to diminish as the number of reusability cycles increases, and this could be attributed to the loss of photocatalyst during the separation process as similarly reported in previous studies [65,66].

3.4. *Scavenging activity percentage of Bi_2O_3 nanorods by DPPH, Nitric oxide (NO), Hydrogen peroxide (HP), and Reducing power (RP) assays*

Antioxidant activities of sample usually vary with the analytical methods used [67] and the evaluation is commonly done using several methods [68]. To generate reliable data and draw reasonable conclusion, more than a single method was adopted for the evaluation of antioxidant potency of the Bi_2O_3 nanorods [69] including 1,1-diphenyl-

Table 1
The comparison of the currently investigated photocatalyst with other photocatalysts on the photodegradation of BG dye.

Photocatalysts	*Dye treated*	*Temp.* (°C)	% degradation	*Refs.*
α-Bi_2O_3	BGBG	25	75*	This study
ZnO nanodisk		25	44.39	[58]
CaO	BG	25	60.1	[59]
CuS	BG	25	39	[60]
Co_3O_4	BG	25	78	[61]
CuS-Cp	BG	25	63	[60]
CuO	BG	25	50	[62]
ZnO nanorods	BGBG	25	64.3	[63]
WO_3/ZnO		25	60.03	[63]

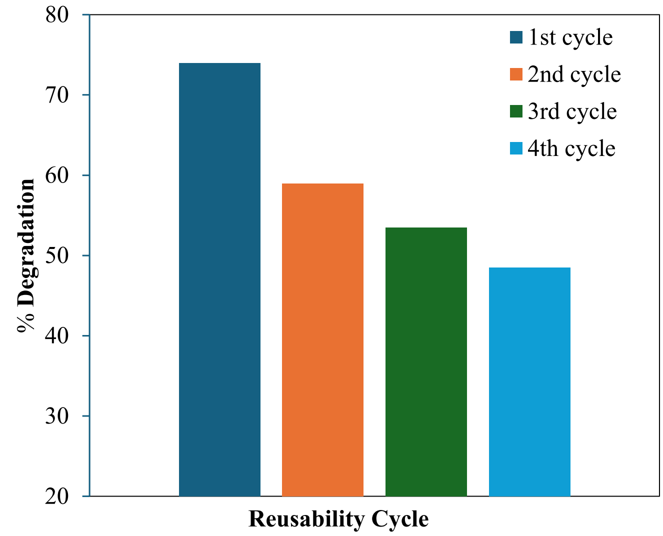

Fig. 9. Reusability cycles of BG using Bi_2O_3 nanorods and BG solution of 20 mg/L.

2-picrylhydrazyle (DPPH), Nitric oxide (NO), Hydrogen peroxide (HP) radical inhibition, and Reducing power (RP) assays. The results of the percentage inhibitions are presented in Table 2 and Fig. 10. The radical inhibition activity of the Bi_2O_3 nanorods was compared with Ascorbic acid (used as standard). In all the assays, Bi_2O_3 nanorods demonstrated a concentration dependent inhibition of radicals with percentage

Table 2
Scavenging activity (%) of Bi_2O_3 nanorods by DPPH, Nitric Oxide (NO), Hydrogen Peroxide (HP), and Reducing power (RP) assays.

Samples	**Concentration (µg/mL)**						**IC50 (µg /mL)**
DPPH	1.56	3.13	6.25	12.5	25	50	
Ascorbic acid	4.43 ± 0.075	12.22 ± 0.036	34.55 ± 0.041	38.04 ± 0.052	50.28 ± 0.060	68.30 ± 0.024	16.25
Bi_2O_3	14.85 ± 0.105	35.79 ± 0.023	35.88 ± 0.045	46.20 ± 0.075	50.59 ± 0.023	55.80 ± 0.009	32.72
Nitric Oxide (NO)							
Ascorbic acid	5.4 ± 0.051	14.54 ± 0.211	33.54 ± 0.054	33.81 ± 0.023	51.75 ± 0.026	72.11 ± 0.056	28.40
Bi_2O_3	13.16 ± 0.037	33.21 ± 0.125	38.94 ± 0.050	48.50 ± 0.015	52.86 ± 0.046	58.73 ± 0.035	29.37
Hydrogen Peroxide (HP)							
Ascorbic acid	6.6 ± 0.033	18.58 ± 0.431	36.59 ± 0.034	36.61 ± 0.054	58.74 ± 0.014	76.17 ± 0.045	25.07
Bi_2O_3	12.12 ± 0.049	28.21 ± 0.022	40.24 ± 0.021	44.56 ± 0.044	60.23 ± 0.012	65.73 ± 0.048	25.22
Reducing power (RP)							
Ascorbic acid	4.80 ± 0.035	22.24 ± 0.032	42.51 ± 0.034	46.24 ± 0.065	60.18 ± 0.026	70.32 ± 0.028	24.50
Bi_2O_3	14.51 ± 0.053	35.26 ± 0.036	38.18 ± 0.071	50.51 ± 0.038	51.87 ± 0.076	60.20 ± 0.025	28.22

Values are expressed as mean inhibition (%) ± Standard deviation (n = 3). Ascorbic acid is a standard.

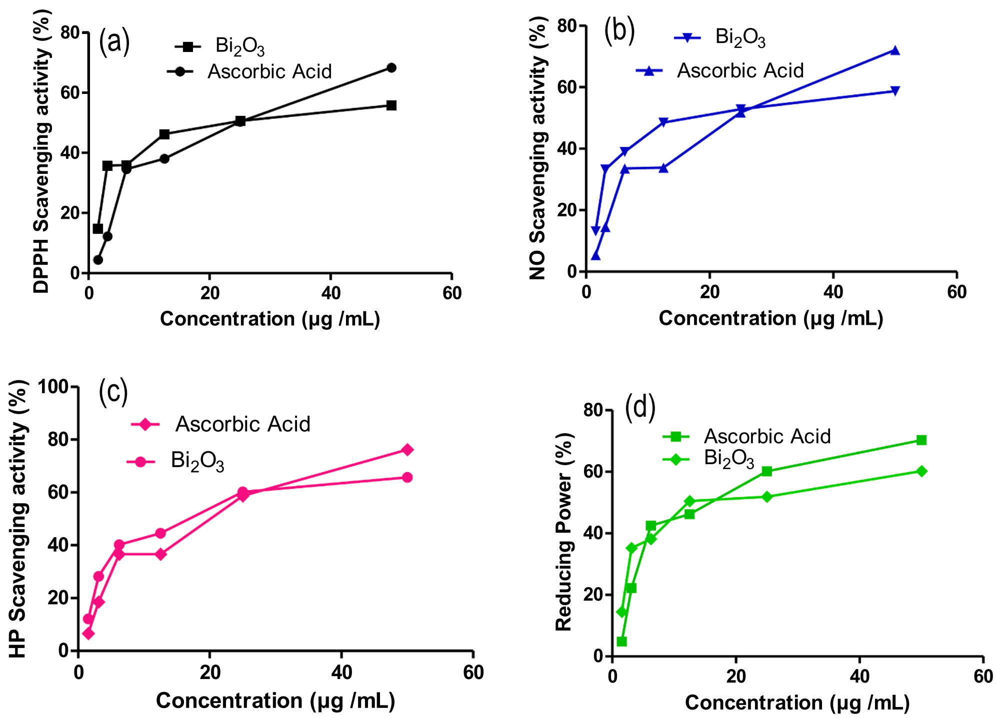

Fig. 10. Scavenging activity (%) of Bi_2O_3 nanorods by DPPH (a), Nitric Oxide (NO) (b), Hydrogen Peroxide (HP) (c), and Reducing power (RP) (d) assays.

efficiency in the range 14.85 ± 0.105 to 55.80 ± 0.009, 13.16 ± 0.037 to 58.73 ± 0.035, 12.12 ± 0.049 to 65.73 ± 0.048 and 14.51 ± 0.053 to 60.20 ± 0.025 for the DPPH, NO, HP radicals, and reducing power assays respectively. Based on the concentrations of Bi_2O_3 nanorods and ascorbic acid that inhibited 50 % of the radicals (IC_{50}), the sample exhibited better inhibition of HP (25.22 µg/mL), followed by RP (28.22 µg/mL), NO (29.37 µg/mL), and DPPH (32.72 µg/mL) respectively , while, the standard Ascorbic acid exhibited IC_{50} values of 16.25, 24.50, 25.07, and 28.40 µg/mL for DPPH, RP, HP, and NO, respectively.

Both Bi_2O_3 nanorods and Ascorbic acid demonstrated similar percentage hydrogen peroxide inhibition as inferred from the IC_{50} values and the results are shown in Fig. 11. There is a paucity of information on the antioxidant activity of Bi_2O_3. However, studies have shown the efficacy as antimicrobial, antihaemolytic, antiplatelet, and anticancer [70–73]. These studies highlighted the effectiveness of Bi_2O_3 in scavenging DPPH radicals with a concentration-dependent decoloration of the purple DPPH to yellow. Ag-Bi_2O_3 and Ag-Bi_2O_3-rGO nanocomposite were also demonstrated to effectively inhibit DPPH radicals compared to the pristine Bi_2O_3. Grigalius and Petrikaite [74] have related anticancer properties of compounds with their antioxidant potency. Antioxidants reduce DNA damage by decreasing free radicals and oxidative stress to prevent cancer developments. In this study, the efficacy of Bi_2O_3 nanorods as antioxidant was validated using the DPPH, NO, HP and RP assays.

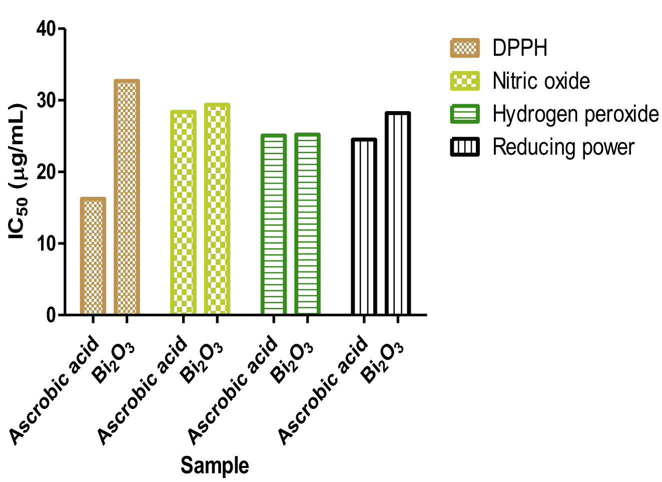

Fig. 11. IC_{50} value for DPPH, Nitric Oxide, Hydrogen Peroxide, and Reducing power inhibition by Bi_2O_3 nanorods and ascorbic acid.

4. Conclusions

Monoclinic Bi_2O_3 were successfully synthesized using a microwave-assisted thermal decomposition route, in which bismuth nitrate was used as a precursor salt and ethylenglycol as solvent. The synthesized bismuth oxides were characterized using different techniques. XRD studies shows that the Bi_2O_3 has a monoclinic structure and crystallized in its α-crystalline phase. Electron microscope studies indicate rod-shaped morphology of the nanoparticles, and the high crystallinity was confirmed by the SAED pattern. UV–visible studies show that the nanorods have strong absorbance in the UV region which also encroaches into the visible region with an absorption peak around 350 nm and band edge around 452 nm, which corresponds to a band gap energy of 2.75 eV. The Bi_2O_3 nanorods have good activity towards the photodegradation of bromocresol green, with an efficiency of about 75 % after 3 h UV light irradiation and an optimum pH of 6. The nanorods were also found to exhibit antioxidant property whose ability to scavenge free radicals across 4 different assays is comparable to Ascorbic acid used as standard. The study successfully demonstrates a short approach towards the synthesis of monoclinic α-Bi_2O_3 of multifunctional application in the environment and biology.

CRediT authorship contribution statement

Marwa Yousry A. Mohamed: Writing – original draft, Methodology, Formal analysis. **Hela Ferjani:** Writing – original draft, Formal analysis, Conceptualization. **Opeyemi A. Oyewo:** Investigation, Formal analysis. **Oluwasayo E. Ogunjinmi:** Validation, Methodology, Formal analysis. **Seham M. Hamed:** Resources. **Chahra Amairia:** Writing –

original draft, Investigation. **Seshibe Makgato:** Resources. **Damian C. Onwudiwe:** Writing – review & editing, Conceptualization.

Declaration of competing interest

The authors declare that they have no known competing financial interests or personal relationships that could have appeared to influence the work reported in this paper.

Data availability

Data will be made available on request.

Acknowledgements

This work was supported and funded by the Deanship of Scientific Research at Imam Mohammad Ibn Saud Islamic University (IMSIU) (grant number IMSIU-RG23126)

References

[1] Y. Liu, L. Zong, C. Zhang, W. Liu, A. Fakhri, V.K. Gupta, Design and structural of Sm-doped SbFeO3 nanopowders and immobilized on poly(ethylene oxide) for efficient photocatalysis and hydrogen generation under visible light irradiation, Surf. Interfaces 26 (2021) 101292.

[2] J. Wang, J. Sun, J. Huang, A. Fakhri, V.K. Gupta, Synthesis and its characterization of silver sulfide/nickel titanate/chitosan nanocomposites for photocatalysis and water splitting under visible light, and antibacterial studies, Mater. Chem. Phys. 272 (2021) 124990.

[3] M.A. Lazar, S. Varghese, S.S. Nair, Photocatalytic water treatment by titanium dioxide: recent updates, Catalysts 2 (2012) 572–601.

[4] C. Medana, P. Calza, F. Dal Bello, E. Raso, C. Minero, C. Baiocchi, Multiple unknown degradants generated from the insect repellent DEET by photoinduced processes on TiO2, J. Mass Spectrom. 46 (2011) 24–40.

[5] B. Lopez-Alvarez, R.A. Torres-Palma, G. Peñuela, Solar photocatalitycal treatment of carbofuran at lab and pilot scale: effect of classical parameters, evaluation of the toxicity and analysis of organic by-products, J. Hazard. Mater. 191 (2011) 196–203.

[6] C.-S. Lu, C.-C. Chen, F.-D. Mai, H.-K. Li, Identification of the degradation pathways of alkanolamines with TiO2 photocatalysis, J. Hazard. Mater. 165 (2009) 306–316.

[7] T. An, J. An, H. Yang, G. Li, H. Feng, X. Nie, Photocatalytic degradation kinetics and mechanism of antivirus drug-lamivudine in TiO2 dispersion, J. Hazard. Mater. 197 (2011) 229–236.

[8] M. Pavel, C. Anastasescu, R.-N. State, A. Vasile, F. Papa, I. Balint, Photocatalytic degradation of organic and inorganic pollutants to harmless end products: assessment of practical application potential for water and air cleaning, Catalysts 13 (2023) 380.

[9] M.B. Tahir, M. Rafique, M.S. Rafique, N. Fatima, Z. Israr, Chapter 6 - Metal oxide- and metal sulfide-based nanomaterials as photocatalysts, in: M.B. Tahir, M. Rafique, M.S. Rafique (Eds.), Nanotechnology and Photocatalysis for Environmental Applications, Elsevier, 2020, pp. 77–96.

[10] H.W. Kim, J.W. Lee, S.H. Shim, Study of Bi2O3 nanorods grown using the MOCVD technique, Sens. Actuators B 126 (2007) 306–310.

[11] L. Leontie, M. Caraman, M. Alexe, C. Harnagea, Structural and optical characteristics of bismuth oxide thin films, Surf. Sci. 507 (2002) 480–485.

[12] A. Gualtieri, S. Immovilli, M. Prudenziati, Powder X-ray diffraction data for the new polymorphic compound ω-Bi2O3, Powder Diffr. 12 (1997) 90–92.

[13] P. Shuk, H.-D. Wiemhöfer, U. Guth, W. Göpel, M. Greenblatt, Oxide ion conducting solid electrolytes based on Bi2O3, Solid State Ion. 89 (1996) 179–196.

[14] R.P. Rao, S. Mishra, R. Tripathi, S.K. Jain, Bismuth oxide nanorods: phytochemical mediated one-pot synthesis and growth mechanism, Inorg. Nano-Metal Chem. (2021) 1–8.

[15] X. Lv, Z. Li, J. Zhang, B. Yang, A facile approach to prepare bismuth oxide nanorods for application in optoelectronic devices, Chem. Lett. 44 (2015) 97–99.

[16] P.R. Solanki, J. Singh, B. Rupavali, S. Tiwari, B.D. Malhotra, Bismuth oxide nanorods based immunosensor for mycotoxin detection, Mater. Sci. Eng. C 70 (2017) 564–571.

[17] X. Huang, W. Zhang, Y. Tan, J. Wu, Y. Gao, B. Tang, Facile synthesis of rod-like Bi2O3 nanoparticles as an electrode material for pseudocapacitors, Ceram. Int. 42 (2016) 2099–2105.

[18] Y. Hanifehpour, B. Mirtamizdoust, J. Dadashi, R. Wang, M. Rezaei, M. Abdolmaleki, S.W. Joo, The synthesis and characterization of a novel one-dimensional bismuth (III) coordination polymer as a precursor for the production of bismuth (III) oxide nanorods, Crystals 12 (2022) 113.

[19] M. Law, H. Kind, B. Messer, F. Kim, P. Yang, Photochemical sensing of NO2 with SnO2 nanoribbon nanosensors at room temperature, Angew. Chem. Int. Ed. 41 (2002) 2405–2408.

[20] X. Wang, X. Zhong, J. Li, Z. Liu, L. Cheng, Inorganic nanomaterials with rapid clearance for biomedical applications, Chem. Soc. Rev. 50 (2021) 8669–8742.

[21] A.A. Mahdi, R.A. Obeid, K. Abdullah, S. Mohammed, A.J. Kadhim, M.F. Ramadan, B.M. Hussien, A. Alkahtani, F.A. Ali, A.G. Alkhathami, L. Al-Fatolahi, A. Fakhri, A facile construction of NiV2O6/CeO2 nano-heterojunction for photo-operated process in water remediation reaction, antibacterial studies, and detection of D-Amino acid in peroxidase system, Surf. Interfaces 40 (2023) 102970.

[22] A. Bahadoran, Q. Liu, B. Liu, J. Gu, D. Zhang, A. Fakhri, V.K. Gupta, Fabrication and structural of gold/cerium nanoparticles on tin disulfide nanostructures and decorated on hyperbranched polyethyleneimine for photocatalysis, reduction, hydrogen production and antifungal activities, J. Photochem. Photobiol. A: Chem. 416 (2021) 113316.

[23] C. Singh, S.K. Anand, R. Upadhyay, N. Pandey, P. Kumar, D. Singh, P. Tiwari, R. Saini, K.N. Tiwari, S.K. Mishra, Green synthesis of silver nanoparticles by root extract of Premna integrifolia L. and evaluation of its cytotoxic and antibacterial activity, Mater. Chem. Phys. 297 (2023) 127413.

[24] A. Marino, M. Battaglini, N. Moles, G. Ciofani, Natural antioxidant compounds as potential pharmaceutical tools against neurodegenerative diseases, ACS Omega 7 (2022) 25974–25990.

[25] J. Flieger, W. Flieger, J. Baj, R. Maciejewski, Antioxidants: Classification, natural sources, activity/capacity measurements, and usefulness for the synthesis of nanoparticles, Materials 14 (2021) 4135.

[26] P. Chen, Y. Li, Y. Dai, Z. Wang, Y. Zhou, Y. Wang, G. Li, Porphyrin-based covalent organic frameworks as doxorubicin delivery system for chemo-photodynamic synergistic therapy of tumors, Photodiagn. Photodyn. Ther. (2024).

[27] N. Motakef-Kazemi, M. Yaqoubi, Green Synthesis and characterization of bismuth oxide nanoparticle using mentha pulegium extract, Iran, J. Pharm. Res. 19 (2020) 70–79.

[28] W. Matysiak, Synthesis of 1D Bi2O3 nanostructures from hybrid electrospun fibrous mats and their morphology, structure, optical and electrical properties, Sci. Rep. 12 (2022) 4046.

[29] M. Zamani, A.M. Delfani, M. Jabbari, Scavenging performance and antioxidant activity of γ-alumina nanoparticles towards DPPH free radical: Spectroscopic and DFT-D studies, Spectrochim. Acta Part A: Mol. Biomol. Spectros. 201 (2018) 288–299.

[30] J.I. García-López, F. Zavala-García, E. Olivares-Sáenz, R.H. Lira-Saldívar, E. Díaz Barriga-Castro, N.A. Ruiz-Torres, E. Ramos-Cortez, R. Vázquez-Alvarado, G. Niño-Medina, Zinc oxide nanoparticles boosts phenolic compounds and antioxidant activity of Capsicum annuum L. during germination, Agronomy 8 (2018) 215.

[31] M.O. Jimoh, A.J. Afolayan, F.B. Lewu, Antioxidant and phytochemical activities of Amaranthus caudatus L. harvested from different soils at various growth stages, Sci. Rep. 9 (2019) 12965.

[32] B. Okeleye, V. Nongogo, N.T. Mkwetshana, R.N. Ndip, Polyphenolic content and in vitro antioxidant evaluation of the stem bark extract of Peltophorum africanum Sond (Fabaceae), Afr. J. Tradit. Complement. Altern. Med. 12 (2015) 1–8.

[33] M. Oyaizu, Studies on Products of Browning Reaction Antioxidative Activities of Products of Browning Reaction Prepared from Glucosamine, The Japanese Journal of Nutrition and Dietetics, 44 (1986) 307-315.

[34] Z. Ai, Y. Huang, S. Lee, L. Zhang, Monoclinic α-Bi2O3 photocatalyst for efficient removal of gaseous NO and HCHO under visible light irradiation, J. Alloy. Compd. 509 (2011) 2044–2049.

[35] S. Singh, R.K. Sahoo, N.M. Shinde, J.M. Yun, R.S. Mane, K.H. Kim, Synthesis of Bi2O3-MnO2 Nanocomposite Electrode for Wide-Potential Window High Performance Supercapacitor, Energies 12 (2019) 3320.

[36] V.S. Vinila, J. Isac, Chapter 14 - Synthesis and structural studies of superconducting perovskite GdBa2Ca3Cu4O10.5+δ nanosystems, in: S. Thomas, N. Kalarikkal, A.R. Abraham (Eds.) Design, Fabrication, and Characterization of Multifunctional Nanomaterials, Elsevier, 2022, pp. 319-341.

[37] A.L.J. Pereira, D. Errandonea, A. Beltrán, L. Gracia, O. Gomis, J. Sans, B. Garcia-Domene, A. Miquel Veyrat, F.J. Manjon, A. Munoz, C. Popescu, Structural study of α-Bi 2 O 3 under pressure, J. Phys. Condens. Matter 25 (2013) 475402.

[38] G. Liu, S. Li, Y. Lu, J. Zhang, Z. Feng, C. Li, Controllable synthesis of α-Bi2O3 and γ-Bi2O3 with high photocatalytic activity by α-Bi2O3→γ-Bi2O3→α-Bi2O3 transformation in a facile precipitation method, J. Alloy. Compd. 689 (2016) 787–799.

[39] J. Hou, C. Yang, Z. Wang, W. Zhou, S. Jiao, H. Zhu, In situ synthesis of α–β phase heterojunction on Bi2O3 nanowires with exceptional visible-light photocatalytic performance, Appl. Catal. B 142–143 (2013) 504–511.

[40] D. Wang, T. Kako, J. Ye, New series of solid-solution semiconductors (AgNbO3) 1–x (SrTiO3) x with modulated band structure and enhanced visible-light photocatalytic activity, J. Phys. Chem. C 113 (2009) 3785–3792.

[41] D. Risold, B. Hallstedt, L.J. Gauckler, H.L. Lukas, S.G. Fries, The bismuth-oxygen system, J. Phase Equilib. 16 (1995) 223–234.

[42] J. Li, Y. Li, G. Zhang, H. Huang, X. Wu, One-dimensional/two-dimensional core–shell-structured Bi2O4/BiO2–x heterojunction for highly efficient broad spectrum light-driven photocatalysis: faster interfacial charge transfer and enhanced molecular oxygen activation mechanism, ACS Appl. Mater. Interfaces 11 (2019) 7112–7122.

[43] P.L. Meena, A.K. Surela, K. Poswal, J.K. Saini, L.K. Chhachhia, Biogenic synthesis of Bi2O3 nanoparticles using Cassia fistula plant pod extract for the effective degradation of organic dyes in aqueous medium, Biomass Convers. Biorefin. (2022) 1–17.

[44] J.M. Berg, A. Romoser, N. Banerjee, R. Zebda, C.M. Sayes, The relationship between pH and zeta potential of∼ 30 nm metal oxide nanoparticle suspensions relevant to in vitro toxicological evaluations, Nanotoxicology 3 (2009) 276–283.

[45] B. Guo, R. Zebda, S.J. Drake, C.M. Sayes, Synergistic effect of co-exposure to carbon black and Fe 2 O 3 nanoparticles on oxidative stress in cultured lung epithelial cells, Part. Fibre Toxicol. 6 (2009) 1–13.

[46] P.K. Dutta, A.K. Ray, V.K. Sharma, F.J. Millero, Adsorption of arsenate and arsenite on titanium dioxide suspensions, J. Colloid Interface Sci. 278 (2004) 270–275.

[47] M. Chadwick, J. Goodwin, E. Lawson, P. Mills, B. Vincent, Surface charge properties of colloidal titanium dioxide in ethylene glycol and water, Colloids Surfaces A: Physicochem. Eng. Aspects 203 (2002) 229–236.

[48] M. Kosmulski, A literature survey of the differences between the reported isoelectric points and their discussion, Colloids Surf. A Physicochem. Eng. Asp. 222 (2003) 113–118.

[49] P. Fernández-Ibáñez, J. Blanco, S. Malato, F. De Las Nieves, Application of the colloidal stability of TiO2 particles for recovery and reuse in solar photocatalysis, Water Res. 37 (2003) 3180–3188.

[50] C.E. Onu, P.E. Ohale, B.N. Ekwueme, I.A. Obiora-Okafo, C.F. Okey-Onyesolu, C. P. Onu, C.A. Ezema, O.O. Onu, Modeling, optimization, and adsorptive studies of bromocresol green dye removal using acid functionalized corn cob, Clean. Chem. Eng. 4 (2022) 100067.

[51] O. Elijah, O. Collins, C. Okonkwo, N.-B. Jessica, Application of modified agricultural waste in the adsorption of bromocresol green dye, Asian J. Chem. Sci. (2020) 15–24.

[52] U. Ghosh, A. Pal, Fabrication of a novel Bi2O3 nanoparticle impregnated nitrogen vacant 2D g-C3N4 nanosheet Z scheme photocatalyst for improved degradation of methylene blue dye under LED light illumination, Appl. Surf. Sci. 507 (2020) 144965.

[53] S. Sood, A. Umar, S.K. Mehta, S.K. Kansal, α-Bi2O3 nanorods: An efficient sunlight active photocatalyst for degradation of Rhodamine B and 2, 4, 6-trichlorophenol, Ceram. Int. 41 (2015) 3355–3364.

[54] G. Gupta, M. Kaur, S.K. Kansal, A. Umar, A.A. Ibrahim, α-Bi2O3 nanosheets: An efficient material for sunlight-driven photocatalytic degradation of Rhodamine B, Ceram. Int. 48 (2022) 29580–29588.

[55] S.P. Patil, V. Shrivastava, G. Sonawane, S. Sonawane, Synthesis of novel Bi2O3–montmorillonite nanocomposite with enhanced photocatalytic performance in dye degradation, J. Environ. Chem. Eng. 3 (2015) 2597–2603.

[56] S. Fassi, K. Djebbar, T. Sehili, Photocatalytic Degegradation of Bromocresol green by TiO2/UV in aqueous medium, J. Mater. Environ. Sci 5 (2014) 1093–1098.

[57] M. Saeed, A. ul Haq, M. Muneer, A. Ahmad, T.H. Bokhari, Q. Sadiq, Synthesis and characterization of Bi2O3 and Ag-Bi2O3 and evaluation of their photocatalytic activities towards photodegradation of crystal violet dye, Phys. Scr. 96 (2021) 125707.

[58] Y.L. Ying, S.Y. Pung, M.T. Ong, Y.F. Pung, Photocatalytic activity of ZnO nanodisks in degradation of Rhodamine B and Bromocresol Green under UV light exposure, J. Phys. Conf. Ser. 1082 (2018) 012085.

[59] J. Osuntokun, D.C. Onwudiwe, E.E. Ebenso, Aqueous extract of broccoli mediated synthesis of CaO nanoparticles and its application in the photocatalytic degradation of bromocrescol green, IET Nanobiotechnol. 12 (2018) 888–894.

[60] A. Nezamzadeh-Ejhieh, N. Moazzeni, Sunlight photodecolorization of a mixture of Methyl Orange and Bromocresol Green by CuS incorporated in a clinoptilolite zeolite as a heterogeneous catalyst, J. Ind. Eng. Chem. 19 (2013) 1433–1442.

[61] M. Honarmand, M. Mahjoore, Sunlight-assisted degradation of bromocresol green using Co3O4 nanoparticles as a High-Performance Photocatalyst, J. Geomine 1 (2023) 7–12.

[62] L. Parimala, J. Santhanalakshmi, CuO nanoparticles with biostabilizers for the catalytic decolorization of bromocresol green, crystal violet, methyl red dyes based on H2O2 in aqueous medium, React. Kinet. Mech. Catal. 109 (2013) 393–403.

[63] Y.L. Ying, S.Y. Pung, M.T. Ong, Y.F. Pung, A comparison study between ZnO Nanorods and WO3/ZnO nanorods in bromocresol green dye removal, Solid State Phenom. 264 (2017) 87–90.

[64] S. Anandan, G.-J. Lee, P.-K. Chen, C. Fan, J.J. Wu, Removal of orange II dye in water by visible light assisted photocatalytic ozonation using Bi2O3 and Au/Bi2O3 nanorods, Ind. Eng. Chem. Res. 49 (2010) 9729–9737.

[65] F. Poorsajadi, M.H. Sayadi, M. Hajiani, M.R. Rezaei, Photocatalytic degradation of methyl orange dye using bismuth oxide nanoparticles under visible radiation, International Journal of New, Chemistry 8 (2021) 229–239.

[66] S.P. Patil, B. Bethi, G. Sonawane, V. Shrivastava, S. Sonawane, Efficient adsorption and photocatalytic degradation of Rhodamine B dye over Bi2O3-bentonite nanocomposites: A kinetic study, J. Ind. Eng. Chem. 34 (2016) 356–363.

[67] K. Guneshwor, A. Haripyaree, Evaluation of antioxidant properties of some herbal plants used as food and medicine, Int. J. Agr. Food Sci. 2 (2012) 127–130.

[68] D. Kuate, B.C.O. Etoundi, Y.B. Soukontoua, J.L. Ngondi, J.E. Oben, Comparative study of the antioxidant, free radical scavenging activity and human LDL oxidation inhibition of three extracts from seeds of a Cameroonian spice, Xylopia parviflora (A. Rich.) Benth. (Annonaceae), Int. J. Biomed. Pharm. Sci 5 (2011) 18–30.

[69] K. Schlesier, M. Harwat, V. Böhm, R. Bitsch, Assessment of antioxidant activity by using different in vitro methods, Free Radic. Res. 36 (2002) 177–187.

[70] C. Stewart, K. Konstantinov, S. McKinnon, S. Guatelli, M. Lerch, A. Rosenfeld, M. Tehei, S. Corde, First proof of bismuth oxide nanoparticles as efficient radiosensitisers on highly radioresistant cancer cells, Phys. Med. 32 (2016) 1444–1452.

[71] M. Sarani, F. Tosan, S.A. Hasani, M. Barani, M. Adeli-Sardou, M. Khosravani, S. Niknam, M.A.J. Kouhbanani, N. Beheshtkhoo, Study of in vitro cytotoxic performance of biosynthesized α-Bi2O3 NPs, Mn-doped and Zn-doped Bi2O3 NPs against MCF-7 and HUVEC cell lines, J. Mater. Res. Technol. 19 (2022) 140–150.

[72] M. Ahamed, M.J. Akhtar, M.M. Khan, H.A. Alhadlaq, Improved antimicrobial and anticancer potential of eco-friendly synthesized Co-doped Bi2O3/RGO nanocomposites, J. Drug Deliv. Sci. Technol. 84 (2023) 104525.

[73] P. Nethravathi, M. Manjula, S. Devaraja, M. Sakar, D. Suresh, Eco-friendly preparation of Bi2O3, Ag-Bi2O3 and Ag-Bi2O3-rGO nanomaterials and their photocatalytic H2 evolution, dye degradation, nitrite sensing and biological applications, J. Photochem. Photobiol. A Chem. 435 (2023) 114295.

[74] I. Grigalius, V. Petrikaite, Relationship between antioxidant and anticancer activity of trihydroxyflavones, Molecules 22 (2017) 2169.